# Theoretical Analysis of Hybrid Plasmonic Waveguide

M. Z. Alam, *Member, IEEE*, J. Stewart Aitchison, *Member, IEEE*, and Mo Mojahedi, *Member, IEEE*

***Abstract*—We investigate the properties of the modes supported by the hybrid plasmonic waveguide consisting of a metal surface separated from a high-index slab by a low-index spacer. We examine the variations of the effective mode indices and field profiles of the hybrid modes for various choices of waveguide dimensions. We show that the observed variations of the modal properties can be explained from the fact that these modes result from the coupling of the surface plasmons, supported by the metal–dielectric interface, and the dielectric waveguide mode, supported by the high-index slab. The method of analysis is very general and can be used to explain the modal properties of the hybrid plasmonic waveguides for a wide range of material properties and waveguide dimensions.**

***Index Terms*—Coupled mode analysis, plasmons, surface waves, waveguides.**

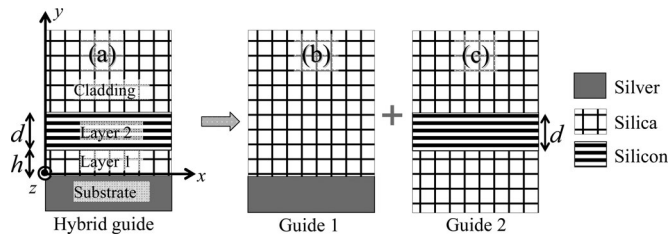


Fig. 1. Hybrid plasmonic waveguide shown in Fig. 1(a) can be considered a combination of two guides: Guide 1 and Guide 2. Guide 1 is a surface plasmon waveguide consisting of silver–silica interface [see Fig. 1(b)], and Guide 2 is a dielectric waveguide consisting of a silicon slab surrounded by silica [see Fig. 1(c)]. Coordinate system used in this study is also shown.

## I. Introduction

SURFACE waves supported by metal–dielectric interface, known as surface plasmons (SP), have attracted a lot of interest in recent years [1]. SP can be useful for many applications such as biosensing [2] and implementation of very compact photonic devices, which are not possible using conventional index guiding methods [3]–[5]. One of the biggest challenges preventing the wide spread use of plasmonics is the significant propagation loss suffered by the SP mode. At optical frequency regime, metal has a complex permittivity and hence SP can propagate only a short distance before the guided power is significantly diminished. In an attempt to obtain a satisfactory compromise between loss and confinement, different plasmonic waveguide designs such as metal–insulator–metal [4], metal slot [6], insulator–metal–insulator [7], channel waveguides [8], and dielectric loaded plasmom guide [9] have been proposed. As an alternative to purely plasmonic waveguides, we have recently proposed a hybrid plasmonic waveguide, which consists of a high-index slab separated from a metal surface with a low-index spacer layer [10]. In this structure, the power is highly concentrated in the low-index spacer layer. Since our first proposal of hybrid plasmonic wave guiding, a number of different kinds of such guides have been investigated [11]–[14] and many practical applications of this guiding scheme have already been suggested [15]–[20]. However, to the best of our knowledge, no detailed investigation has been carried out to explain the guiding mechanism of the hybrid guide. Although [10]–[14] have studied some of the hybrid mode characteristics and have stated that the hybrid mode is formed from the coupling of the SP and dielectric waveguide modes, no detailed analysis was provided to support this idea. This lack of a detailed analysis has led to some confusion. For example, some recent work has pointed out the absence of quasi-odd modes in the previously reported hybrid guiding schemes as evidence against the mode hybridization in such structures [21]. A detailed analysis of the modes supported by the hybrid plasmonic guide under various conditions will clarify the physical nature of the guided modes in these structures and the better understanding thus achieved may also be useful for the design of future hybrid plasmonic waveguide devices. The purpose of this study is to carry out such an analysis.

This paper is organized as follows. In Section II, we describe the hybrid plasmonic waveguide and methods of analysis followed in this study. In Section III, we investigate the variations of effective mode indices and field profiles for the guided modes with variations of waveguide dimensions. To keep the problem analytically solvable, we consider only 1-D structure. In Section IV, we summarize the modal characteristics and show that these characteristics can be explained from the assumption that the modes supported by the hybrid plasmonic guides result from the coupling of the SP and dielectric waveguide modes. Section V concludes this paper with some remarks.

## II. Description of Structure and the Method of Analysis

The geometry of the metal-low–high-index guides is shown in Fig. 1(a). It consists of a silicon slab (layer 2) of thickness $d$ separated from a silver surface by a silica layer (layer 1) of thickness $h$. The structure is invariant in the $x$- and $z$-directions.

The silica region separating the silver surface from silicon is designated as spacer throughout this study. The cladding is

Manuscript received August 3, 2012; revised November 20, 2012 and December 14, 2012; accepted December 18, 2012. This work was supported by the Natural Sciences and Engineering Research Council of Canada (NSERC) Strategic Network for Bioplasmonic Systems (BiopSys), Canada, under Grant 486537.

The authors are with the Department of Electrical and Computer Engineering, University of Toronto, Toronto, ON, M5R 0A3, Canada (e-mail: muhammad.alam@mail.utoronto.ca; stewart.aitchison@utoronto.ca; mojahedi@waves.utoronto.ca).

Color versions of one or more of the figures in this paper are available online at http://ieeexplore.ieee.org.

Digital Object Identifier 10.1109/JSTQE.2013.2238894

also silica. Permittivities of the silver, silica, and silicon are $\varepsilon_{\mathrm{Ag}}, \varepsilon_{\mathrm{Silica}}$, and $\varepsilon_{\mathrm{Si}}$, respectively.

In general, coupled, i.e., hybrid modes can be either TE or TM type but since the SP mode supported by Guide 1 is TM in nature, the hybrid modes supported by the structure shown in Fig. 1(a) can also be only TM type [10]. Therefore, we consider only the TM modes in this study. Modes supported by the structure can be analyzed using the transfer matrix method since it can provide accurate solutions for the modes supported by a 1-D multilayered structure. The method works by constructing the propagation and interface matrixes as explained in detail in [22]. Assuming propagation in the $z$-direction, the expressions for the magnetic fields for the intermediate layer $j$ ($j = 1, 2$) can be written as

$$\vec{H}_j(y,z) = \hat{x}H_{xj}(y)\exp[i(\gamma z - \omega t)]. \tag{1}$$

Here, $\gamma = k_0(N_{\mathrm{eff}} + iK_{\mathrm{eff}})$ is the complex propagation constant, $k_0 = (2\pi)/\lambda_0$ is the free space wave number, $\lambda_0$ is the free space wavelength, and finally $N_{\mathrm{eff}}$ and $K_{\mathrm{eff}}$ are the real and imaginary parts of the effective refractive index.

The magnetic field in the cladding $\vec{H}_c$ and in the substrate $\vec{H}_s$ can be expressed as

$$\vec{H}_c(y,z) = \hat{x}A_c e^{-k_c(y-(h+d))}\exp[i(\gamma z - \omega t)] \tag{2}$$

$$\vec{H}_s(y,z) = \hat{x}A_s e^{k_s y}\exp[i(\gamma z - \omega t)] \tag{3}$$

where $k_s$ and $k_c$ define the rate of attenuation in the substrate (silver) and cladding (silica) and are given by

$$k_s = \sqrt{\gamma^2 - \varepsilon_{\mathrm{Ag}}k_0^2} \tag{4}$$

$$k_c = \sqrt{\gamma^2 - \varepsilon_{\mathrm{Silica}}k_0^2}. \tag{5}$$

The electric field in various layers can be obtained from the magnetic field by the application of Maxwell's curl equations. By using the boundary condition of tangential electric field and magnetic field at the various interfaces, the dispersion relation for the multilayer structure can be obtained as

$$\frac{k_s}{\varepsilon_{\mathrm{Ag}}}m_{11} + \frac{k_c}{\varepsilon_{\mathrm{Silica}}}m_{22} - m_{21} - \frac{k_s k_c}{\varepsilon_{\mathrm{Ag}}\varepsilon_{\mathrm{Silica}}}m_{12} = 0. \tag{6}$$

The coefficients $m_{i,j}$ ($i = 1, 2$; $j = 1, 2$) are given by

$$\begin{bmatrix} m_{11} & m_{12} \\ m_{21} & m_{22} \end{bmatrix} = \begin{bmatrix} \cos(k_1 h) & -\dfrac{\varepsilon_{\mathrm{Silica}}}{k_1}\sin(k_1 h) \\ \dfrac{k_1}{\varepsilon_{\mathrm{Silica}}}\sin(k_1 h) & \cos(k_1 h) \end{bmatrix} \times \begin{bmatrix} \cos(k_2 d) & -\dfrac{\varepsilon_{\mathrm{Si}}}{k_2}\sin(k_2 d) \\ \dfrac{k_2}{\varepsilon_{\mathrm{Si}}}\sin(k_2 d) & \cos(k_2 d) \end{bmatrix}. \tag{7}$$

Here, $k_j$ is the transverse wave number for the $j$th layer ($j = 1, 2$) and is given by

$$k_1 = \sqrt{\varepsilon_{\mathrm{Silica}}k_0^2 - \gamma^2} \tag{8}$$

$$k_2 = \sqrt{\varepsilon_{\mathrm{Si}}k_0^2 - \gamma^2}. \tag{9}$$

Solutions of (6) provide accurate information about the guided modes for any combinations of waveguide dimensions and material properties. However, getting a physical picture of the mode formation from this approach is not a straightforward task. The concept of coupled mode, although approximate can provide better physical insight. The hybrid plasmonic waveguide can be thought of as a combination of two waveguides as shown in Fig. 1. Guide 1 is an SP waveguide formed by a silver–silica interface [see Fig. 1(b)], where as Guide 2 is a high-index contrast dielectric waveguide formed by a silicon slab surrounded by silica [see Fig. 1(c)]. For a small spacer thickness coupling between these two guides will be very strong. Results obtained from the conventional coupled mode theory (CMT) are valid only for weakly coupled structures [23]. On the other hand, nonorthogonal CMT can provide satisfactory results in the case of strong coupling but only for low-index contrast guides [24]. Therefore, straight forward application of neither the conventional CMT nor the nonorthogonal CMT can provide accurate results about the mode characteristics for such cases [25]. However, this does not mean that the coupled modes are not formed in the structure shown in Fig. 1(a). As long as the difference in effective indices of the modes supported by the Guides 1 and 2 is small and the guides are in close vicinity, coupled modes will be formed. In this paper, we use the dispersion relation [see (6)] to find the exact solutions for the guided modes but rely on the concept of coupling among the modes to provide a physical picture of the modes formation. We examine the properties of the modes supported by the hybrid structure for various silicon and spacer layer thicknesses at 1.55-$\mu$m wavelength. The permittivity of silica and silicon is taken from [26], and that of silver is taken from [27]. Equation (6) is solved by the function fminsearch from MATLAB's Optimization Toolbox to find the allowed modes. This function uses the simplex search algorithm that is simple, and does not require the computation of numerical or analytical gradients; however, it can find only local solutions. To ensure that we are indeed calculating the effective mode indices properly, we compared the values obtained by solving (6) with those obtained from the finite-element code, Comsol Multiphysics. The effective indices predicted by the two methods matched well and the difference was less than 0.03% in the worst case.

## III. Properties of the Modes Supported by the Hybrid Plasmonic Guide

In case of coupling between two identical waveguides, one of the coupled modes exhibits even symmetry and the other one exhibits odd symmetry with respect to the midpoint of the gap region (spacer) separating the two guides. In case of coupling between two dissimilar waveguides (the case discussed in this study), the coupled modes lack complete symmetry but as shown later in this section, one of the modes is still "quasi-even" (does not become zero anywhere in the spacer region) and the other mode is "quasi-odd" (becomes zero somewhere in the spacer region). Behavior of the modes supported by the hybrid plasmonic waveguide depends strongly on the properties of the modes supported by the Guides 1 and 2. Therefore, an

TABLE I
NOTATIONS USED IN THIS STUDY AND THEIR MEANINGS

| Symbol | Meaning |
|---|---|
| $N_{SP}^{G1}$ | Real part of the effective mode index for the SP supported by Guide 1 |
| $N_{TM0}^{G2}$ | Real part of effective mode index of $TM_0$ mode supported by Guide 2 |
| $N_{TM1}^{G2}$ | Real part of effective mode index of $TM_1$ mode supported by Guide 2 |
| $N_{Even}^{HG}$ | Real part of the effective mode index of the quasi-even mode supported by the hybrid guide |
| $N_{Odd}^{HG}$ | Real part of the effective mode index of the quasi-odd mode supported by the hybrid guide |
| $\Delta_0 = N_{TM0}^{G2} - N_{SP}^{G1}$ | Difference between the real parts of the effective mode indices for the $TM_0$ mode supported by Guide 2 and SP mode supported by Guide 1 |
| $\Delta_1 = N_{TM1}^{G2} - N_{SP}^{G1}$ | Difference between the real parts of the effective mode indices for the $TM_1$ mode supported by Guide 2 and SP mode supported by Guide 1 |
| $D_{TM1}^{Cut}$ | Cut off thickness for $TM_1$ mode of Guide 2 |

TABLE II
VARIOUS CONDITIONS INVESTIAGTED IN THIS STUDY

| Case # | Condition | Silicon thickness ($d$) | Difference between effective mode indices |
|---|---|---|---|
| 1 | $N_{SP}^{G1} > N_{TM0}^{G2}$, Small $\Delta_0$, $d << d_{TM1}^{Cut}$ | 45 nm | $\Delta_0$= - 0.0026 |
| 2 | $N_{SP}^{G1} = N_{TM0}^{G2}$, Small $\Delta_0$, $d << d_{TM1}^{Cut}$ | 50.8 nm | $\Delta_0$=0 |
| 3 | $N_{SP}^{G1} < N_{TM0}^{G2}$, Small $\Delta_0$, $d << d_{TM1}^{Cut}$ | 100 nm | $\Delta_0$= 0.0426 |
| 4 | $N_{SP}^{G1} < N_{TM0}^{G2}$, Large $\Delta_0$, $d << d_{TM1}^{Cut}$ | 130 nm | $\Delta_0$= 0.1 |
| 5 | $N_{SP}^{G1} < N_{TM0}^{G2}$, Large $\Delta_0$, $d \approx< d_{TM1}^{Cut}$ | 240 nm | $\Delta_0$= 0.764 |
| 6 | $N_{SP}^{G1} < N_{TM1}^{G2}$, Small $\Delta_1$, Large $\Delta_0$, $d > d_{TM1}^{Cut}$ | 340 nm | $\Delta_0$= 1.346; $\Delta_1$= 0.0344 |

examination of the modes supported by Guides 1 and 2 is needed before we proceed further. The notations used in this discussion are shown in Table I. Guide 1 supports only one mode: SP at the silver/silica interface, while the number of modes supported by Guide 2 and their behavior depend on silicon thickness $d$; however, for $d < 250$ nm, Guide 2 supports only $TM_0$ mode.

Depending on the silicon thickness, a number of different situations are possible. The conditions which may arise for silicon thickness up to 340 nm ($0 < d \leq 340$ nm) are summarized in Table II. For large film thickness higher order modes (for example, $TM_2$ mode) may also be supported that are not considered in our analysis. However, careful investigation of the cases mentioned in Table II enables us to easily predict the mode characteristics for such cases and therefore, we refrain from discussing those cases. For very large silicon thickness, the hybrid plasmonic waveguide converts to a conductor-gap-dielectric waveguide that has been discussed in detail in [21].

In the following, we investigate the behavior of the hybrid waveguide modes with varying silicon and spacer thicknesses subject to the constraints enumerated in Table II. In some of the cases in addition to the hybrid mode, dielectric waveguide modes supported by the silicon slab also exists independently. For example, in case 6 ($d = 340$ nm) in addition to modes whose profiles are combinations of modes supported by Guide 1 and Guide 2, a mode also exists which is almost identical to the $TM_0$ mode supported by Guide 2. These dielectric waveguide modes are well studied and well understood, and hence will not be investigated here.

### A. Variations of the Effective Mode Index

Fig. 2(a), (b), and (c) shows the variations of $N_{\mathrm{Even}}^{\mathrm{HG}}$ with varying spacer thickness ($h$) for the cases of Table II. Variations of $N_{\mathrm{Even}}^{\mathrm{HG}}$ and $N_{\mathrm{Odd}}^{\mathrm{HG}}$ for cases 1 and 2 are very similar and to avoid redundancy, case 2 is omitted in these plots. The solid lines are

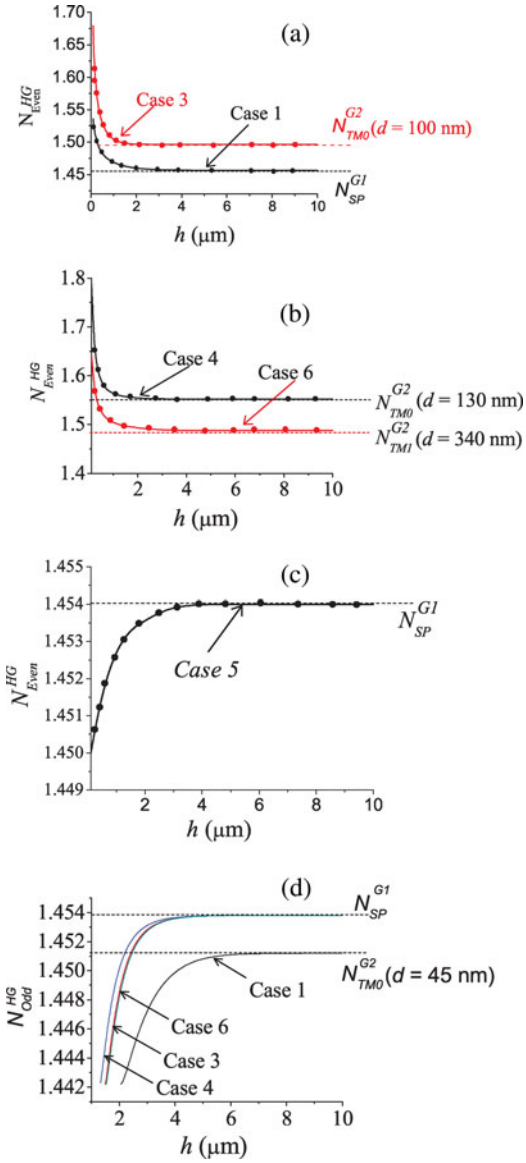


Fig. 2. Variations of effective mode indices for the guided modes as a function of $h$ (spacer height) for various $d$ (silicon thickness). (a), (b), and (c) are for quasi-even and (d) is for quasi-odd.

obtained by an analytical method [solving (6)], and the circles indicate the results from Comsol Multiphsycis. Variations of $N^{\mathrm{HG}}_{\mathrm{Odd}}$ for various cases are plotted in Fig. 2(d). Although the agreement between the analytical method and Comsol Multiphysics is also good in this case, to avoid crowding the plot, only results obtained from the analytical method are shown in Fig. 2(d). The quasi-even mode exists for any $h$ but quasi-odd mode is cutoff for small $h$. For cases 1 and 2 ($N^{G1}_{\mathrm{SP}} \geq N^{G2}_{\mathrm{TM0}}$), for increasing spacer thickness $(h)$, $N^{\mathrm{HG}}_{\mathrm{Even}}$ approaches $N^{G1}_{\mathrm{SP}}$ and $N^{\mathrm{HG}}_{\mathrm{Odd}}$ approaches $N^{G2}_{\mathrm{TM0}}$. For cases 3 and 4, for increasing $h$, in contrast to cases 1 and 2, $N^{\mathrm{HG}}_{\mathrm{Even}}$ approaches $N^{G2}_{\mathrm{TM0}}$ and $N^{\mathrm{HG}}_{\mathrm{Odd}}$ approaches $N^{G1}_{\mathrm{SP}}$.

For the case 5 ($d = 240$ nm), hybrid mode characteristics are significantly different from the other cases in Table II. In this case, the guide does not support quasi-odd mode for any spacer thickness, and as shown in Fig. 2(c), the variation of

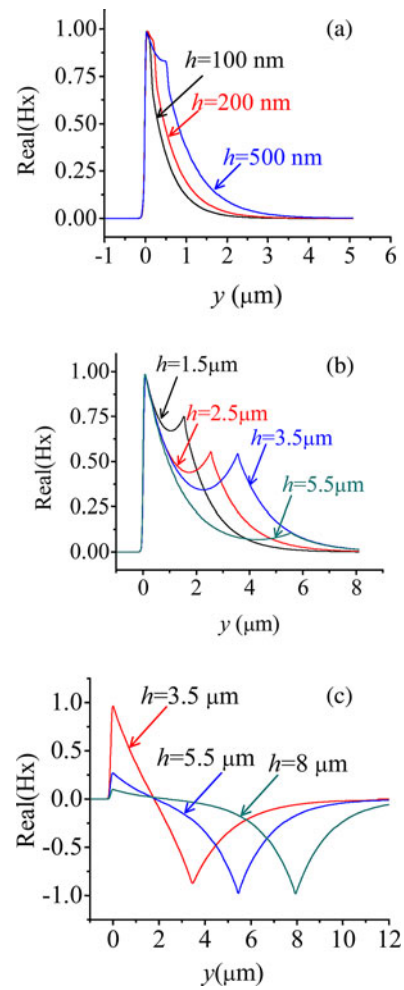


Fig. 3. (a) and (b) Real part of the normalized magnetic field for the quasi-even mode. (c) Real part of the normalized magnetic field for the quasi-odd mode. In all figures $h$ is the spacer thickness and silicon thickness $d$ is 45 nm. (Case 1 of Table II)

$N^{\mathrm{HG}}_{\mathrm{Even}}$ is opposite of that of quasi-even mode in other cases, i.e., with increasing $h$, $N^{\mathrm{HG}}_{\mathrm{Even}}$ increases instead of decreasing. For the case 6 ($d = 340$ nm), Guide 2 is multimode. In this case, $N^{\mathrm{HG}}_{\mathrm{Even}}$ approaches $N^{G2}_{\mathrm{TM1}}$ and $N^{\mathrm{HG}}_{\mathrm{Odd}}$ approaches $N^{G1}_{\mathrm{SP}}$. It is interesting to note that variations of the effective indices for case 3 ($d = 100$ nm) and case 6 ($d = 340$ nm) are very similar. The reason for this is explained in Section IV.

### B. Variations of Field Profile With Spacer Thickness

In this section, we examine the effects of varying the spacer thickness $h$, for a fixed silicon thickness $d$, on the field profiles for the cases considered in Table II. We plot the real part of the transverse magnetic field $H_x$. To properly designate the nature of the hybrid mode, we use the following notations. If the hybrid mode is formed from the coupling of SP mode supported by the Guide 1 and $\mathrm{TM}_0$ mode supported by the Guide 2, and if with increasing the spacer thickness $h$ the mode converts to an SP mode supported by the Guide 1, we designate it as SP–$\mathrm{TM}_0$. If on the other hand, the mode converts to a TM0 mode supported by the Guide 2, we designate it as $\mathrm{TM}_0$–SP. A similar nomenclature is used for other cases (e.g., SP–$\mathrm{TM}_1$ or $\mathrm{TM}_1$–SP). Fig. 3(a)

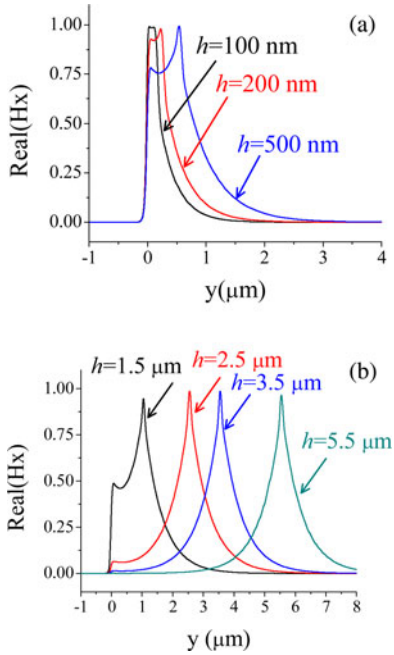


Fig. 4. Real part of the normalized magnetic field for the quasi-even mode for varying spacer thicknesses $h$. Silicon thickness $d$ is 100 nm. (Case 3 of Table II).

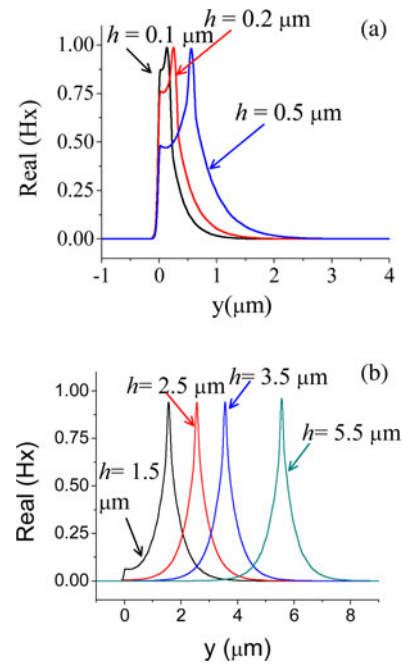


Fig. 5. Real part of the normalized magnetic field for the quasi-even mode for varying spacer thicknesses $h$. Silicon thickness $d$ is 130 nm. (Case 4 of Table II).

through (c) shows the evolution of quasi-even and quasi-odd modes for varying spacer thickness $h$ for the case 1 of Table II ($d = 45$ nm). Here, $y = 0$ is the position of the silver/silica interface. To show the mode profiles clearly for both small and large $h$, we have plotted the mode profiles of quasi-even mode in two different figures, i.e., Fig. 3(a) and (b). As can be seen from these figures, quasi-even mode is of the type SP–$TM_0$ and quasi-odd mode is of the type $TM_0$–SP. For the case 2 of the Table II ($h = 50.8$ nm), the mode profiles and their evolution with varying spacer thickness are very similar to those of the case 1 and are not discussed here. To keep the discussion brief, we will plot the field profiles only for the quasi-even mode for the rest of the cases and summarize the properties of both quasi-even and quasi-odd modes at the end of this section. Increasing silicon film thickness changes the nature of the mode. For the case 3 in Table II ($d = 100$ nm) in contrast to cases 1 and 2, the quasi-even mode is of the type $TM_0$–SP as shown in Fig. 4. The quasi-odd mode is of the type SP–$TM_0$ (not shown in the figure). A further increase in the silicon film thickness $d$ makes $\Delta_0$ larger and the mode begins to lose its hybrid nature. As an example, Fig. 5 shows the mode profiles for the case 4 of the Table II ($d = 130$ nm). The quasi-even mode in this case is concentrated in the silicon slab and is similar to the $TM_0$ mode supported by Guide 2 and with increasing spacer thickness it very quickly converts to $TM_0$ mode supported by Guide 2. For larger silicon thickness (greater than case 4 but smaller than case 5) the coupling becomes less significant, i.e., the quasi-even mode and quasi-odd modes very closely resembles $TM_0$ mode of Guide 2 and SP mode of Guide 1, respectively. For an even larger silicon thickness, e.g., case 5 of Table II ($d = 240$ nm), the silicon slab supports a $TM_0$ mode that is weakly affected by presence of the metal and is not large enough to

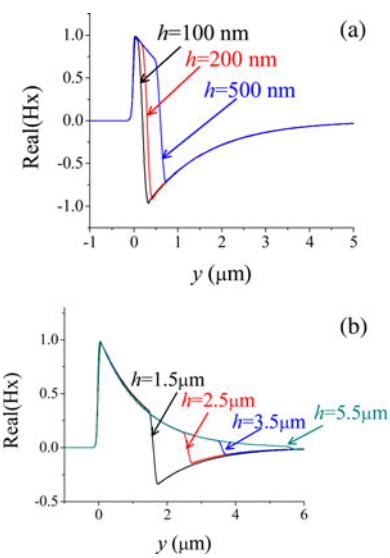


Fig. 6. Real part of the normalized magnetic field for the quasi-even mode for varying spacer thicknesses $h$. Silicon thickness $d$ is 240 nm. (Case 5 of Table II).

support a $TM_1$ mode when surrounded by silica on both sides, the hybrid mode is still the result of coupling between SP and $TM_1$ mode. The mode is of type SP–$TM_1$, i.e., it converts to SP mode for larger spacer thickness. Quasi-odd mode is not supported in this case for any spacer thickness.

With further increase in the silicon thickness (e.g., case 6 in Table II, $d = 340$ nm), Guide 2 becomes multimode and supports both $TM_0$ and $TM_1$ modes. Similar to the case 5, SP couples with the $TM_1$ mode and the resulting quasi-even mode is of the type $TM_1$–SP, as shown in Fig. 7. It should be pointed out that although the field profiles in Figs. 6 and 7 may seem to resemble quasi-odd modes, the magnetic field $H_x$ in fact does not cross

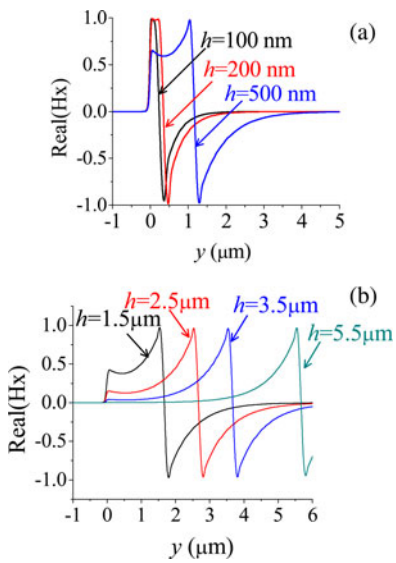


Fig. 7. Real part of the normalized magnetic field for the quasi-even mode for varying spacer thicknesses $h$. Silicon thickness $d$ is 340 nm. (Case 6 of Table II).

TABLE III
SUMMARY OF MODAL CHARACTERISTICS FOR THE CASES OF TABLE II

| Case # | Nature of quasi-even mode | Nature of the quasi-odd mode |
|---|---|---|
| 1 | SP-$TM_0$ | $TM_0$-SP |
| 2 | SP-$TM_0$ | $TM_0$-SP |
| 3 | $TM_0$-SP | SP-$TM_0$ |
| 4 | $TM_0$-SP | SP-$TM_0$ |
| 5 | SP – $TM_1$ | Does not exist |
| 6 | $TM_1$-SP | SP-$TM_1$ |

zero in the spacer but inside the silicon film. The modes shown in Figs. 6 and 7, therefore, are quasi-even modes and not quasi-odd. For case 6, the quasi-odd modes of the type SP-$TM_1$ are also present for large spacer that are not shown in the figure. Table III summarizes the mode types for the various cases of Table II.

## IV. Summary and Analysis of the Hybrid Plasmonic Waveguide Modes

There are several general trends related to the mode formations in the hybrid plasmonic waveguide that can be arrived at from our discussion in Section III. In the following, we will list these trends and provide some physical explanations underlying the observed behaviors.

1) The quasi-even mode of the hybrid plasmonic waveguide exists for any spacer thickness $h$, but the quasi-odd mode is cutoff for small spacer thickness.
   As stated in Section I, the presence of only one mode in the hybrid guide for small spacer thickness has led some researchers to question the validity of the mode hybridization concept in these waveguides [21]. However, it must be pointed out that some assumptions of the conventional CMT such as the weakly coupling condition and orthogonality of the guided modes are not necessary valid for the hybrid plasmonic waveguides in which the separation between the constituent waveguides (Guides 1 and 2) is extremely small. In fact, *nonorthogonal* CMT formulation predicts that the quasi-odd modes reach the cutoff condition for small waveguides separation [23], which is illustrated for the hybrid waveguides examined here. Since [10]–[14] considered only small spacer thickness, the odd mode was absent for the hybrid plasmonic guides considered in those work.
2) For increasing spacer thickness the hybrid modes convert to the modes guided by the constituent waveguides (Guides 1 and 2). The quasi-even mode always converts to the mode of Guide 1 or 2, whichever has a higher effective mode index. Quasi-odd mode on the other hand, converts to the mode of Guide 1 or 2, whichever has a lower effective mode index.
   This behavior is expected when coupling takes place between two nonidentical waveguides as has been explained in more detail in [28].
3) If Guide 2 supports multiple modes, SP mode supported by the Guide 1 couples to the dielectric waveguide mode supported by the Guide 2 whose effective index is closest to its own effective index.
   This is consistent with the concept of coupled mode formation: only modes with comparable effective indices are expected to couple and form hybrid modes.
4) Hybrid mode of type SP–$TM_1$ exists even when $d < D_{\mathrm{TM1}}^{\mathrm{Cut}}$ provided that $\left|d - D_{\mathrm{TM1}}^{\mathrm{Cut}}\right|$ is small. The quasi-odd mode is absent in this case {case 5 of Table II}.
   The situation is very similar to the asymmetrical nanoscale plasmonic waveguide reported in [29]. As shown in [29], if a plasmonic (metallic) slot waveguide is placed on a dielectric substrate, the metal blocks the radiation away from the slot waveguide and the cutoff width of the guide is reduced. A similar explanation also holds for the case 5 {of Table II}. The presence of the metal near the high-index slab in a hybrid waveguide acts as a strong reflector and cutoff thickness of the $TM_1$ mode is reduced. Hence, a hybrid mode of the type SP–$TM_1$ is formed even when the silicon slab is below the cutoff thickness of the $TM_1$ mode ($d < D_{\mathrm{TM1}}^{\mathrm{Cut}}$). For large spacer thickness $h$, the effect of reflection from the metal surface is less pronounced and the silicon slab fails to support the $TM_1$ mode. Hence, quasi-odd mode does not exist even for large $h$.
5) Hybrid mode characteristics can be very similar for very different silicon thicknesses. This is illustrated in Fig. 2. For the cases 3 and 6 {of Table II} the variations of $N_{\mathrm{Even}}^{\mathrm{HG}}$ and $N_{\mathrm{Odd}}^{\mathrm{HG}}$ and the cutoff thickness of the quasi-odd mode are very similar, although the silicon thicknesses for the two cases are 100 and 340 nm, respectively.

This behavior can also be explained using the concept of coupled modes. In the case 3, the hybrid mode results from coupling of the SP mode and the $TM_0$ mode. As shown in Table II, the difference between the effective mode indices of the constituent modes $\Delta_0$ is 0.0426. In the case 6, coupling occurs between the SP mode and the $TM_1$ mode, and the difference between the effective indices in this case $\Delta_1$ is 0.0344, which is close to that of the case 3. Therefore, variations of the effective mode indices ($N_{\mathrm{Even}}^{\mathrm{HG}}$ and $N_{\mathrm{Odd}}^{\mathrm{HG}}$) and also the cutoff thicknesses for the quasi-odd mode for the two cases are also similar.

## V. Conclusion

In this paper, we have investigated the properties of the modes supported by the hybrid plasmonic guide for various choices of waveguide dimensions. We have shown that the characteristics of these modes can be explained by assuming that they result from the coupling of SP and dielectric waveguide modes. The analysis presented in this study can be important in the design of hybrid plasmonic waveguide devices and choosing suitable excitation mechanism for these devices. For most practical applications, single mode conditions are preferred. Relatively thin silicon film and small spacer thickness should be chosen for ensuring single mode condition for those applications. The hybrid mode can be excited using end fire, prism, or grating in these cases. Multimode waveguide can also be useful for some applications, for example, in biosensing [30]. Large spacer thickness will be suitable for such cases. Prism or grating coupling can be used for exciting multiple modes for these applications.

To keep the analysis simple, we have considered only symmetric condition, i.e., same materials for both cover and spacer layer in this study. Although we have not presented results for the asymmetric cases, for example, for air cover and silica spacer, the physical picture presented here remains valid also for those cases. Detailed analyses of asymmetric structures will be reported in the future.

## References


[1] W. L. Barnes, A. Dereux, and T. W. Ebbesen, "Surface plasmon subwavelength optics," *Nature*, vol. 424, pp. 824–830, 2003.

[2] J. Homola, "Present and future of surface plasmon resonance biosensors," *Anal. Bional. Chem.*, vol. 377, pp. 528–539, 2003.

[3] J. Takahara, S. Yamagishi, H. Taki, A. Morimoto, and T. Kobayashi, "Guiding of a one-dimensional optical beam with nanometer diameter," *Opt. Lett.*, vol. 22, pp. 475–477, 1997.

[4] J. A. Dionne, L. A. Sweatlock, and H. A. Atwater, "Plasmon slot waveguides: Towards chip-scale propagation with subwavelength-scale localization," *Phys. Rev. B*, vol. 73, art. no. 035407, 2006.

[5] J. A. Dionne, L. A. Sweatlock, M. T. Sheldon, A. P. Alivisatos, and H. A. Atwater, "Silicon-based plasmonics for on-chip photonics," *IEEE J. Sel. Top. Quantum Electron.*, vol. 16, no. 1, pp. 295–306, Jan./Feb. 2010.

[6] G. Veronis and S. Fan, "Guided subwavelength plasmonic mode supported by a slot in thin metal film," *Opt. Lett.*, vol. 30, pp. 3359–3361, 2005.

[7] P. Berini, "Long-range surface plasmon polaritons," *Adv. Opt. Photon.*, vol. 1, pp. 484–588, 2009.

[8] S. I. Bozhevolnyi, V. S. Volkov, E. Devaux, J. Y. Laluet, T. W. Ebbesen, "Channel plasmon subwavelength waveguide components including interferometers and ring resonators," *Nature,* vol. 440, pp. 508–511, 2006.

[9] B. Steinberger, A. Hohenau, H. Ditlbacher, A. L. Stepanov, and A. Dretz, "Dielectric stripe on gold as surface plasmon waveguides," *Appl. Phys. Lett.*, vol. 88, art. no. 094104, 2006.

[10] M. Z. Alam, J. Meier, J. S. Aitchison, and M. Mojahedi. (2007). "Super mode propagation in low index medium," *CLEO/QELS*. [Online]. Available: http://www.opticsinfobase.org/abstract.cfm?uri=CLEO-2007-JThD112

[11] R. F. Oulton, V. J. Sorger, D. A. Genov, D. F. P. Pile, and X. Zhang, "A hybrid plasmonic waveguide for subwavelength confinement and long range propagation," *Nature Photon.*, vol. 2, pp. 496–500, 2008.

[12] M. Fujii, J. Leuthold, and W. Freude, "Dispersion relation and loss of subwavelength confined mode of metal-dielectric-gap optical waveguides," *IEEE Photon. Tech. Lett.*, vol. 21, no. 6, pp. 362–364, Mar. 15, 2009.

[13] D. Dai and S. He, "A silicon-based hybrid plasmonic waveguide with a metal cap for a nano-scale light confinement," *Opt. Exp.*, vol. 17, pp. 16646–16653, 2009.

[14] M. Z. Alam, J. Meier, J. S. Aitchison, and M. Mojahedi, "Propagation characteristics of hybrid modes supported by metal-low-high index waveguides and bends," *Opt. Exp.*, vol. 18, pp. 12971–12979, 2010.

[15] M. Z. Alam, J. S. Aitchison, and M. Mojahedi, "Compact and silicon-on-insulator-compatible hybrid plasmonic TE-pass polarizer," *Opt. Lett.*, vol. 37, pp. 55–57, 2012.

[16] M. Z. Alam, J. S. Aitchison, and M. Mojahedi, "Compact hybrid TM-pass polarizer for silicon-on-insulator platform," *Appl. Opt.*, vol. 50, pp. 2294–2298, 2011.

[17] M. Z. Alam, J. S. Aitchison, and M. Mojahedi, "A polarization independent hybrid plasmonic coupler for silicon on insulator platform," *Opt. Lett.*, vol. 37, pp. 3417–3419, 2012.

[18] R. F. Oulton, V. J. Sorger, T. Zentgraf, R. M. Ma, C. Gladden, L. Dai, Bartal, and X. Zhang, "Plasmon lasers at deep subwavelength scale," *Nature*, vol. 461, pp. 629–632, 2009.

[19] M. Z. Alam, F. Bahrami, J. S. Aitchison, and M. Mojahedi, "A hybrid waveguide sensor for highly sensitive biosensing," CLEO paper ID: JWA111, 2011.

[20] F. F. Lu, T. Li, X. P. Hu, Q. Q. Cheng, S. N. Zhu, and Y. Y. Zhu, "Efficient second harmonic generation in nonlinear plasmonic waveguides," *Opt. Lett.*, vol. 36, pp. 3371–3373, 2011.

[21] I. Avrutsky, R. Soref, and W. Buchwald, "Sub-wavelength plasmonic modes in a conductor-gap-dielectric system with nanoscale gap," *Opt. Exp.*, vol. 18, pp. 348–363, 2010.

[22] I. G. Breukelaar, "Surface plasmon-polaritons in thin metal strips and slabs: Wave guiding and mode cutoff," Master Thesis, School Inf. Technol. Eng., University of Ottawa, Ottawa, Canada, 2004.

[23] A. Hardy and W. Streifer, "Coupled mode theory for parallel waveguides," *J. Lightw. Technol.*, vol. 3, no. 5, pp. 1135–1146, Oct. 1985.

[24] W. Snyder, A. Ankiewicz, and A. Atlintas, "Fundamental error of recent coupled mode formulations," *Eletron. Lett.*, vol. 23, pp. 1097–1098, 1987.

[25] M. L. Cooper and S. Mookherjea, "When and how coupled-mode theory fails in high-index contrast arrayed and multi-slot waveguides," *CLEO/QELS*, paper ID JThE94, 2009.

[26] E. D. Palik, *Handbook of Optical Constants of Solids*. Orlando, FL, USA: Academic, 1985.

[27] P. B. Johnson and R. W. Christy, "Optical constants of noble metals," *Phys. Rev. B*, vol. 6, pp. 4370–4379, 1972.

[28] H. A. Haus and W. Huang, "Coupled-mode theory," *Proc. IEEE*, vol. 79, no. 10, pp. 1505–1518, Oct. 1991.

[29] N. Berkovich, M. Orenstein, and S. G. Lipson, "Novel complex modes in asymmertical nanoscale plasmonic waveguides," *Opt. Exp.*, vol. 16, pp. 17842–17847, 2008.

[30] M. Weisser, B. Menges, and S. M-Neher, "Refractive index and thickness determination of monolayers by multi-mode waveguide coupled surface plasmons," *Sens. Act. B*, vol. 56, pp. 189–197, 1999.



**M. Z. Alam** (S'10–M'13) received the B.Sc. Engineering degree from the Bangladesh University of Engineering and Technology, Dhaka, Bangladesh, in 2000, the MA.Sc. degree from the University of Victoria, Victoria, Canada, in 2004, and the Ph.D. degree from the University of Toronto, Toronto, Canada, in 2012.

He is currently a Postdoctoral Fellow in the Photonics Group at the University of Toronto. His research interests include plasmonics, integrated optics, electromagnetics, biosensing, and optical gas sensing.

**J. Stewart Aitchison** (M'96) received the B.Sc. (First Class Hons.) and the Ph.D. degrees from the Physics Department, Heriot-Watt University, Edinburgh, U.K., in 1984 and 1987, respectively. His Ph.D. dissertation research was focused on optical bistability in semiconductor waveguides.

From 1988 to 1990, he was a Postdoctoral Member of Technical Staff at Bellcore, Red Bank, NJ, USA, where his research interests included high nonlinearity glasses and spatial optical solitons. He then joined the Department of Electronics and Electrical Engineering, University of Glasgow, in 1990 and was promoted to a Personal Chair as a Professor of Photonics in 1999. His research focused on the use of the half-bandgap nonlinearity of semiconductors for the realization of all-optical switching devices and the study of spatial soliton effects. He was also involved in the development of quasi-phase matching techniques in semiconductors, monolithic integration, optical rectification, and planar silica technology. His research group developed novel optical biosensors, waveguide lasers, and photosensitive direct writing processes-based around the use of flame hydrolysis deposited silica. In 1996, he was the holder of the Royal Society of Edinburgh Personal Fellowship and carried out research on spatial solitons as a Visiting Researcher at the Center for Research and Education in Optics and Lasers, University of Central Florida. Since 2001, he has held the Nortel Chair in Emerging Technology in the Department of Electrical and Computer Engineering, University of Toronto, Toronto, Canada. His current research interests include all-optical switching and signal processing, plasmonics, optoelectronic integration, and optical biosensors.

Dr. Aitchison is a Fellow of the Optical Society of America, a Fellow of the Institute of Physics London, a Fellow of the American Association for the Advancement of Science and a Fellow of the Royal Society of Canada. He was awarded the Wallace Prize for best overall performance in his undergraduate class.

**Mo Mojahedi** (S'97–M'98) received the Ph.D. degree from the Center for High Technology Materials (CHTM), University of New Mexico (UNM), Albequerque, USA, in December 1999.

Immediately after receiving the Ph.D. degree, he was a Research Assistant Professor with the CHTM. Since August 2001, he has been with the Faculty of the Electrical and Computer Engineering, University of Toronto, Toronto, ON, Canada. His research interests include matter wave interactions, plasmonics, integrated optics, metamaterials, dispersion engineering, quantum dots, and wells lasers, fundamental electromagnetic theory.

Dr. Mojahedi received the Popejoy Award for the outstanding doctoral dissertation in physics and engineering at UNM during 1997–2000.